Supporting Information Appendix

SI Text

Spectroscopic Details. Low temperature absorption data were collected on a Cary-17 spectrometer using a Janis Research Super Vari-Temp cryogenic Dewar mounted in the optical path. MCD measurements were performed on Jasco J810 (UV/vis, S1 and S20 PMT detection) and J730 (NIR,liquid N2-cooled InSb detection) spectropolarimeters equipped with an Oxford Instruments SM4000-7T superconducting magnet/cryostats. The MCD spectra were corrected for the natural CD and zero-field baseline effects caused by glass strain by averaging the positive and negative field data at 5 K ([7T - (-)7T]/2). Samples of ~1 mM Cu_A-containing protein in ammonium acetate buffer (pH 5.5) for wt Cu_A azurin and M123X (X=Q, L, H) mutants were diluted with glycerol-*d*3 (~50% v/v) and injected into sample cells composed of two quartz disks separated by a Viton O-ring spacer. The concentrations of the protein were determined by EPR spin quantitation. Resonance Raman (RR) spectra were obtained by collecting scattered light dispersed through a triple monochromator (Spex 1877 CP, with 1,200, 1,800, and 2,400 grooves/millimeter holographic spectrograph gratings) and detecting with an Andor Newton charge-coupled device (CCD) detector cooled to -80 °C. Excitation was provided by a Coherent Innova Sabre 25/7 Ar^+ CW ion laser (476.5 nm, ~20 mW). The spectral resolution was ~2 cm^{-1}. The samples were cooled to 77 K in a quartz liquid nitrogen (LN_2) finger dewar (Wilmad). EPR spectra were obtained by using a Bruker EMX spectrometer, ER 041 XG microwave bridge, and ER 4102ST cavity. All X band samples were run at 77 K in a LN_2 finger dewar. A Cu^{2+} standard (1.0 mM $CuSO_4 \bullet 5H_2O$ with 2 mM HCl and 2 M $NaClO_4$) was used for spin quantitation of the EPR spectra.

Computational Details. The DFT models were taken directly from either X-ray structures of the engineered Cu_A Az (PDB ID: 1CC3) or BC (PDB ID: 4AZU). For Cu_A, these consist of protein the backbone loop connecting the to two bridged S(Cys) residues as well as the equatorial N(His) residues and the corresponding axial residues for WT and M123X (X=Q, L, H) mutants. Geometry optimizations were calculated using the hybrid B3LYP exchange-correlation functional with tight SCF convergence criteria (10^{-8} au) and mixed triple-ζ/double-ζ (TZVP on Cu, S, N and 6-31G* on the other atoms) basis sets (1-3). Partial geometry optimizations were performed with the positions of the protein backbone C, N, and O atoms frozen to the X-ray structure positions. Ionization energies (IEs) have been calculated using the difference in total SCF energy (PCM corrected, ε = 4.0) between the fully optimized reduced and oxidized structures. The IE's are related to E^0 by: E^0 (eV) = IE – 4.5 + U, where -4.5 eV converts vacuum to the normal hydrogen electrode, and U is the solvation term. Only IEs relative to WT Cu_A Az are reported. For the calculation of axial bond strength and λ_i for Cu_A and BC, the constrained S(Met) residue was replaced by dimethyl thioether. The $[(Im)(S(CH_3)_2)Cu(SCH_3)_2Cu(Im)(CH_3CONHCH_3)]$ Cu_A model was used for the time-dependent DFT (TD-DFT) calculated excited state slopes (energies and intensities of the 30 lowest-energy, spin-allowed electronic transitions were calculated). For the calculated absorption spectra energies and intensities were transformed with the SWizard program into simulated spectra using Gaussians with full-width half-maxima of 1350 cm^{-1} (4). All

DFT calculations were performed using the program Gaussian 03/09 in the spin-unrestricted formalism (5). EPR spin Hamiltonian parameters were calculated using the ORCA program with hybrid functional B3LYP and the CoreProp basis set for Cu and the SVP basis set for other atoms. These basis sets are the TurboMole DZ basis sets developed by Ahlrichs and coworkers and were obtained from the basis set library (6-9).

References

1. Perdew JP (1986) Density-functional approximation for the correlation energy of the inhomogeneous electron gas *Phys. Rev. B* 33:8822-8824.
2. Becke AD (1988) Density-functional exchange-energy approximation with correct asymptotic behavior *Phys. Rev. A* 38:3098-3100.
3. Becke AD (1993) Density-functional thermochemistry III. The role of exact exchange *J. Chem. Phys. 98*:5648-5653.
4. Gorelsky SI (1999) *SWizard*; Department of Chemistry, York University: Toronto, ON, http://www.sg-chem.net.
5. Frisch, M. J.; *Gaussian 03*, revision C.02; Gaussian, Inc.: Wallingford, CT, 2004.
6. Neese F ORCA, version 2.5; Universität Bonn: Bonn, Germany. The program is available free of charge at http://www.thch.uni-bonn.de/tc/orca.
7. Neese F (2002) Prediction and interpretation of the ^{57}Fe isomer shift in Mössbauer spectra by density functional theory *Inorg Chim Acta* 337:181–192.
8. Schäfer A, Horn H, & Ahlrichs R (1992) Fully optimized contracted Gaussian basis sets for atoms Li to Kr *J Chem Phys* 97:2571–2577.
9. See: ftp.chemie.unikarlsruhe.de/pub/basen
10. Hwang HJ & Lu Y (2004) pH-dependent transition between delocalized and trapped valence states of a Cu_A center and its possible role in proton-coupled electron transfer. *Proc Natl Acad Sci USA* 101(35):12842-12847.

(A)

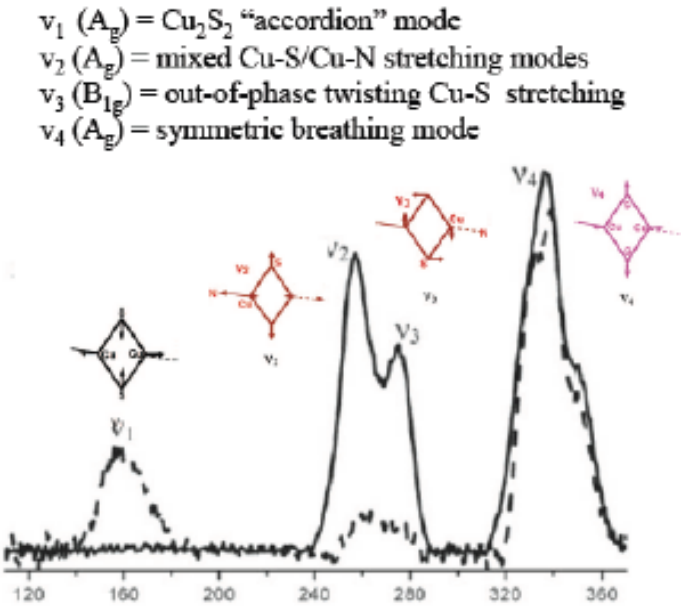

(B)

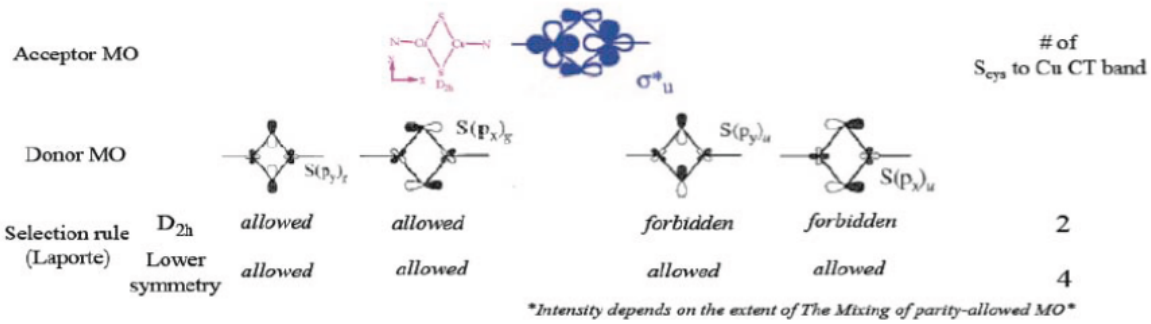

Fig. S1. Schematic representation for: (A) the symmetry of the four vibration modes associated with the [Cu_2S_2] core, and (B) the selection rules for S_{Cys} to Cu CT bands in D_{2h} and lower molecular symmetry.

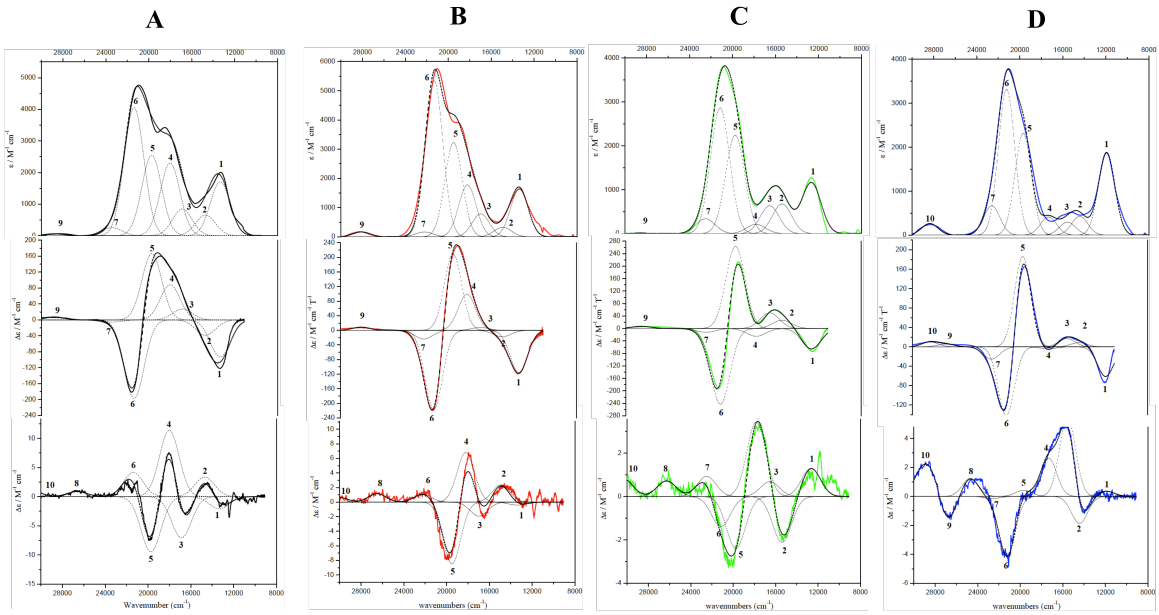

Fig. S2. The LT Abs/MCD/CD spectra of (A) WT (B) M123Q (C) M123L (D) M123H and the peaks are resolved by simultaneous fitting.

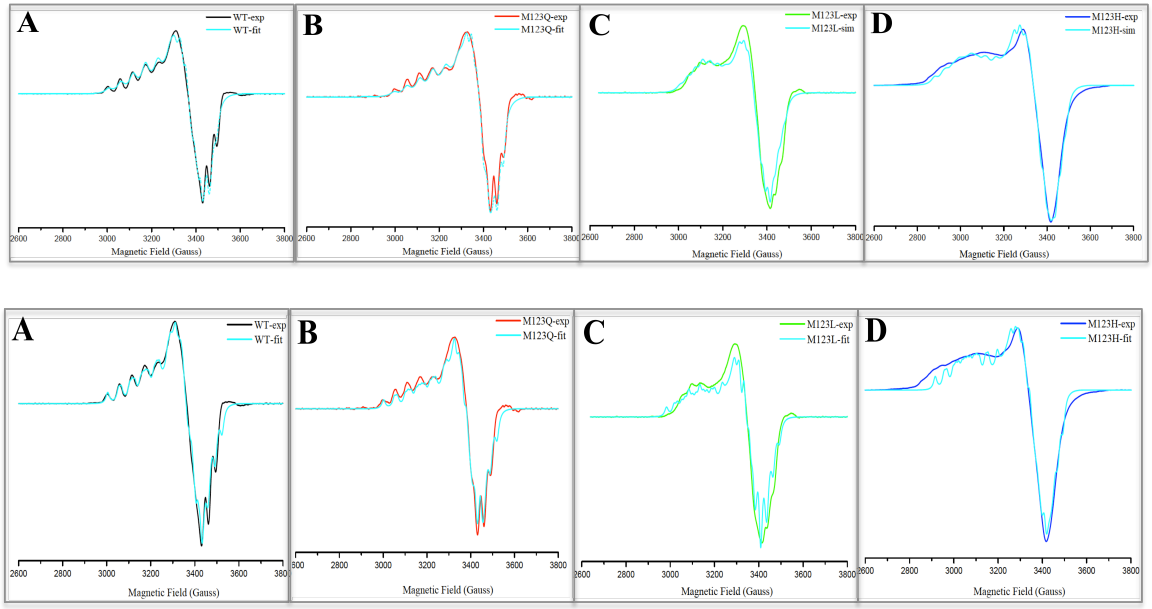

Fig. S3. Overlay of experimental and simulated EPR spectra of (A) WT; (B) M123Q; (C) M123L; and (D) M123H. Top and Bottom show two different simulations. Top: simulation allowed for the bandwidth of A-values to float. Bottom: The bandwidth of A-values are fixed. Parameters from the simulations are given in Table S2.

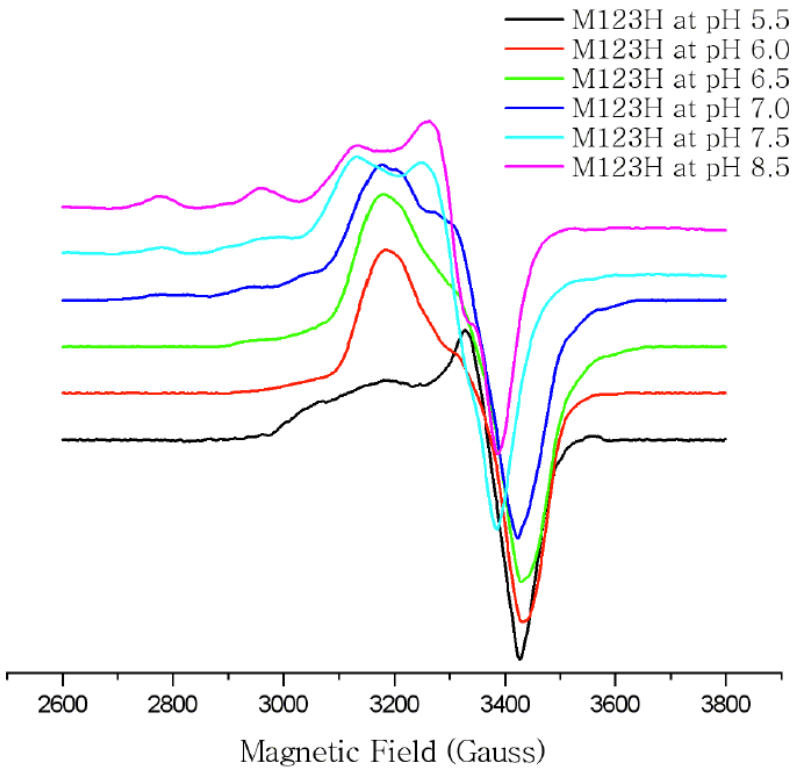

Fig. S4. pH-dependent X-band EPR spectra of the M123H variant. Note that WT Cu_A azurin transforms into a type 2 Cu site at pH ~8.5. (Purple spectrum, Ref 10)

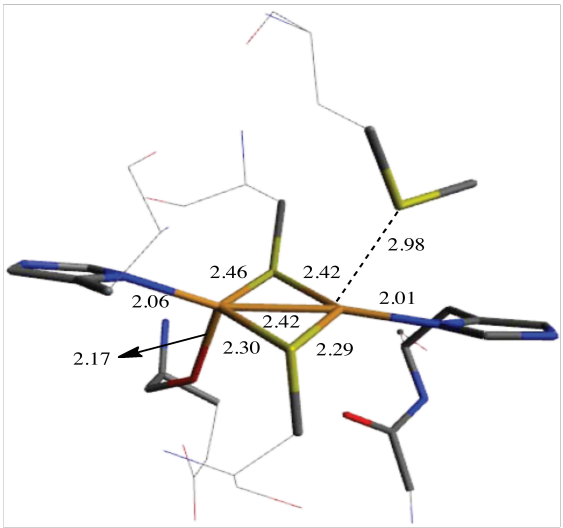

Fig. S5. Schematic representation of the 1.65 Å resolution X-ray structure of engineered Cu_A azurin (PDB ID: 1CC3).

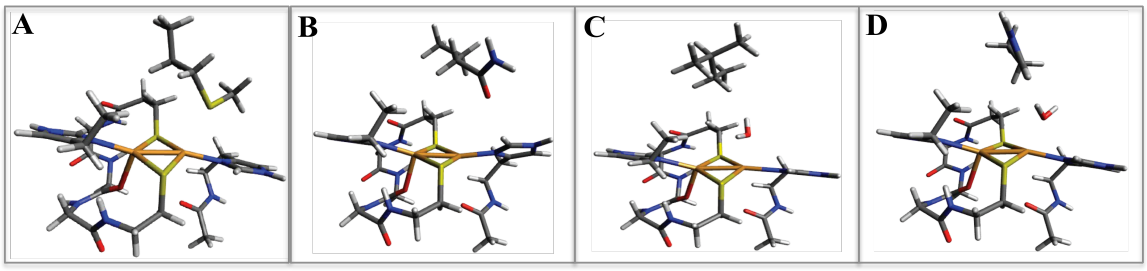

Fig. S6. Schematic representation for DFT-optimized structures: (A) WT; (B) M123Q; (C) M123L; and (D) M123H.

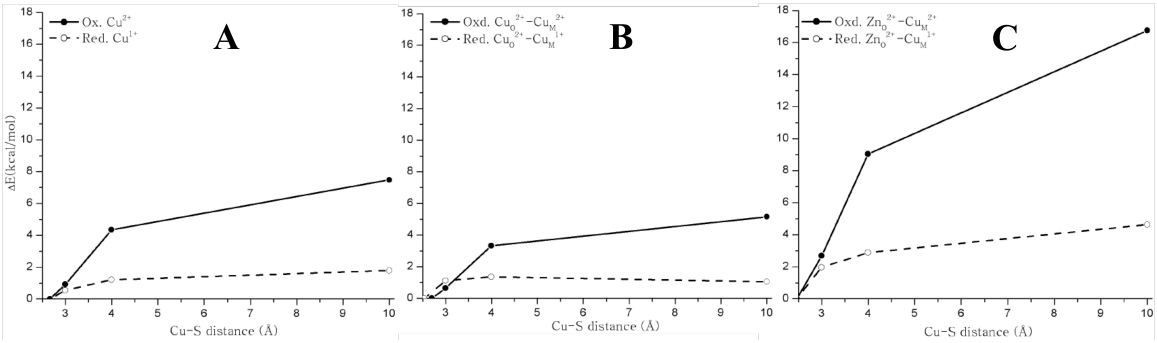

Fig. S7. PESs as a function of Cu-S(thioether) distance for: (A) blue copper; (B) delocalized [Cu_O-Cu_M]; and (C) localized [Zn_O-Cu_M]. Solid line, oxidized Cu site; dashed line, reduced Cu site.

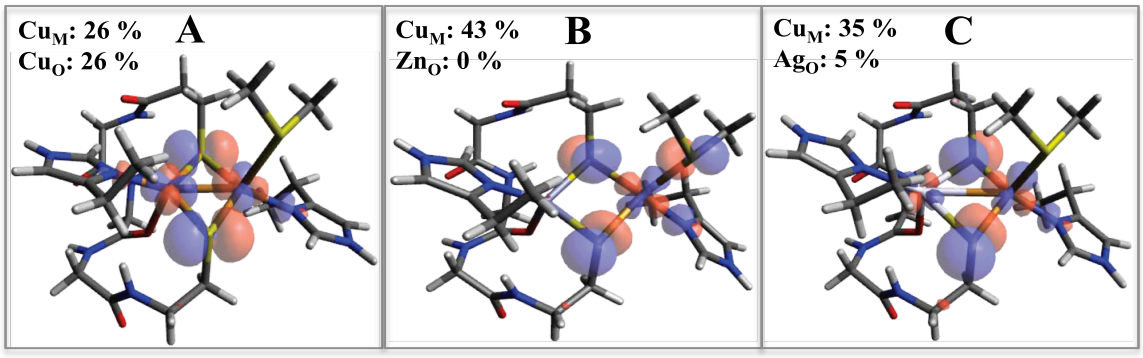

Fig. S8. The orbital populations and β-LUMO contours for (A) [$Cu^{1.5+}$-$Cu^{1.5+}$]; (B) [Zn^{2+}-Cu^{2+}]; and (C) [Ag^{1+}-Cu^{2+}] models.

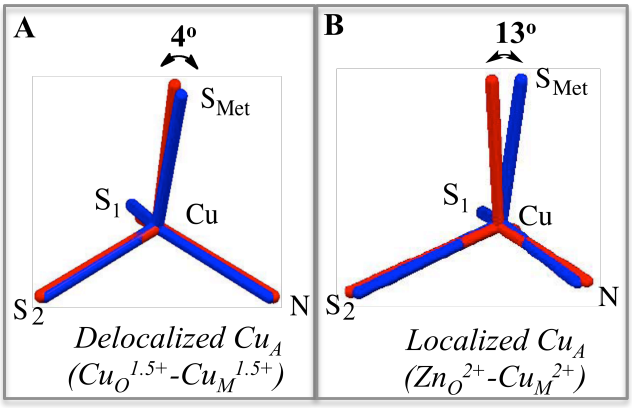

Fig. S9. Overlays of reduced (red) and oxidized (blue) Cu_A DFT structures for: (A) delocalized [Cu_O-Cu_M] and (B) localized [Zn_O-Cu_M] (only Cu and coordinated N, S atoms are shown for clarity). The arrows indicate a rotation of the angle between the S(Met)-Cu-S_1(Cys) and N(His)-Cu-S_2(Cys) planes.

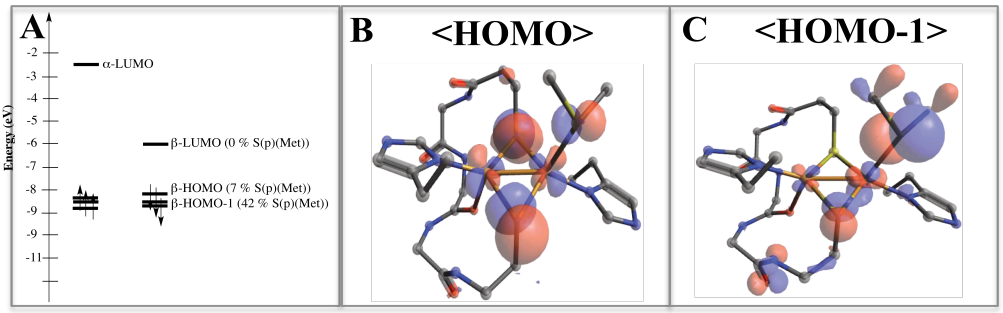

Fig. S10. Energy diagram (A) and selected orbital contours of the HOMO (B) and HOMO-1 (C) of the σ_u* ground state.

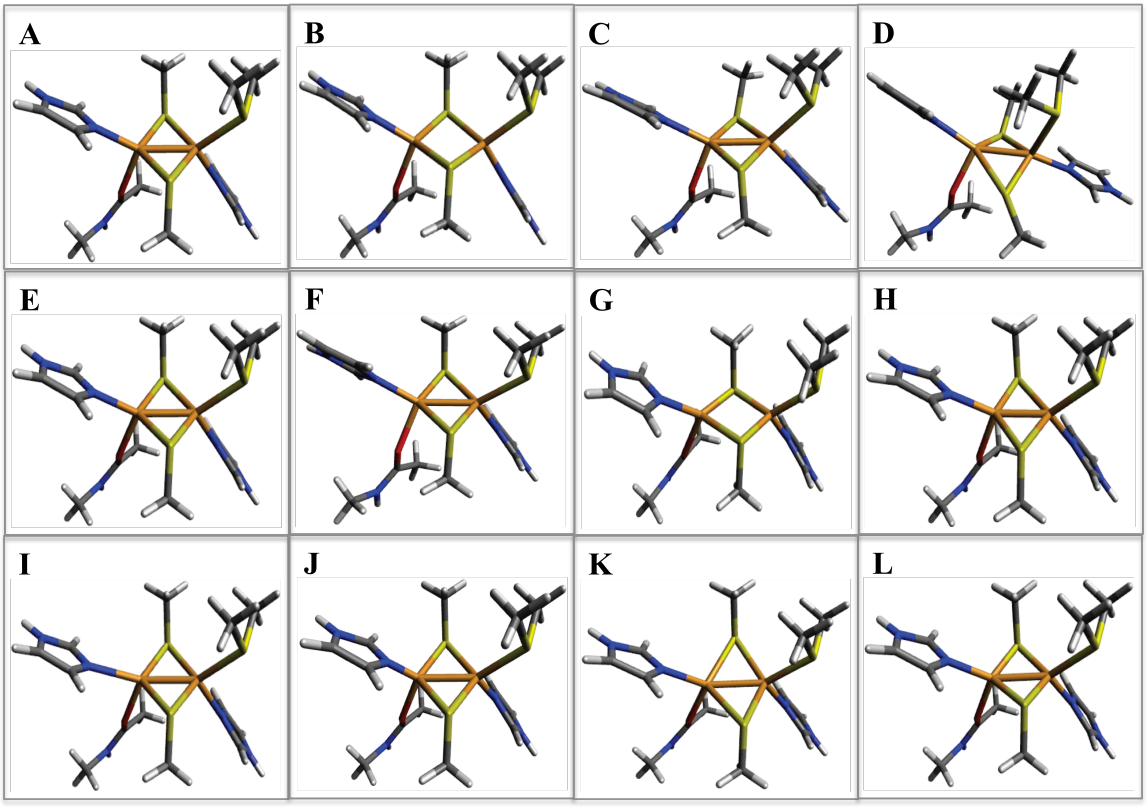

Fig. S11. Various starting structures for geometric optimizations: (A) Cu-Cu: 2.5 Å; (B) Cu-Cu: 3.2 Å; (C) Cu-S(Cys)-Cu-S(Cys) dihedral angle: 0°; (D) Cu-S(Cys)-Cu-S(Cys) dihedral angle: 30°; (E) N(His)-Cu-Cu-N(His) dihedral angle: -180°; (F) N(His)-Cu-Cu-N(His) dihedral angle: -150°; (G) accordion distortion of $[Cu_2S_2]$ with long Cu-Cu distance: Cu-Cu: 3.3 Å; S-S: 2.9 Å; (H) accordion distortion of $[Cu_2S_2]$ with short Cu-Cu distance: Cu-Cu: 2.3 Å; S-S: 4.0 Å; (I) long Cu-N(His): 2.4 Å in average; (J) short Cu-N(His): 1.5 Å in average; (K) long Cu-S(Cys): 2.6 Å in average; and (L) long Cu-S(Cys): Å

Table S1. The absorption and MCD parameters of resolved electronic transitions for: (A) WT; (B) M123Q; (C) M123L; and (D) M123H.

(A)

WT								
band	1	2	3	4	5	6	7	9
Energy (cm^{-1})	13347	14714	16880	18014	19730	21379	23448	28835
ε (M^{-1} cm^{-1})	1706	655	846	2299	2548	4053	255	61
Δε (M^{-1} cm^{-1} T^{-1})	-92	-38	28	88	166	-198	-6	8
C_0/D_0	0.054	0.058	0.034	0.038	0.066	0.048	0.024	0.132

(B)

M123Q								
band	1	2	3	4	5	6	7	9
Energy (cm^{-1})	13369	14918	16973	18211	19505	21312	22232	28092
ε (M^{-1} cm^{-1})	1651	330	789	1780	3229	5345	168	169
Δε (M^{-1} cm^{-1} T^{-1})	-116	-18	8	98	210	-218	-24	8
C_0/D_0	0.07	0.054	0.010	0.056	0.066	0.04	0.142	0.048

(C)

M123L								
band	1	2	3	4	5	6	7	9
Energy (cm^{-1})	12658	15391	16540	17816	19753	21161	22513	28567
ε (M^{-1} cm^{-1})	1162	679	635	213	2245	2867	340	10
Δε (M^{-1} cm^{-1} T^{-1})	-66	26	50	-26	264	-242	-12	8
C_0/D_0	0.056	0.038	0.078	0.122	0.108	0.084	0.036	0.8

(D)

M123H								
band	1	2	3	4	5	6	7	10
Energy (cm^{-1})	11930	14432	15560	17334	19687	21230	22606	28367
ε (M^{-1} cm^{-1})	1880	425	297	412	2318	3320	668	265
Δε (M^{-1} cm^{-1} T^{-1})	-60	8	18	-4	186	-142	-24	10
C_0/D_0	0.032	0.018	0.06	0.010	0.085	0.042	0.036	0.038

Table S2. Simulations of the spin Hamiltonian parameters of WT Cu_A Az and the M123X (X=Q, L, H) variants.

	g_z	g_x	g_y	A_z^{Cu1}	A_z^{Cu2}	A_x^{Cu1}	A_x^{Cu2}	A_y^{Cu1}	A_y^{Cu2}
1*				(10^{-4} cm^{-1})		(10^{-4} cm^{-1})		(10^{-4} cm^{-1})	
WT	2.177	2.022	2.022	53	53	25	27	25	26
M123Q	2.174	2.022	2.027	61	57	21	29	14	19
M123L	2.215	2.004	2.057	35	35	22	21	23	18
M123H	2.255	2.017	2.066	58	42	23	22	22	30
2*									
WT	2.177	2.008	2.043	63	50	27	31	10	24
M123Q	2.174	2.008	2.033	64	50	25	30	15	20
M123L	2.215	2.018	2.047	40	53	29	29	16	20
M123H	2.255	2.014	2.064	46	52	26	18	30	19

*1 and 2 correspond to simulations shown in Figure S3 Top and Bottom, respectively.

Table S3. Selected geometric parameters of Cu_A Az (PDB ID: 1CC3) and calculated WT and M123X (X=Q, L, H) DFT models.

	Cu-L_{axial}*	Cu-Cu	Cu_M-N(His)	Cu_O-N(His)	Cu_M-S(Cys)†	Cu_O-S(Cys)†
WT-exp	2.98	2.42	2.04	2.06	2.36	2.38
WT	2.95	2.49	2.02	2.04	2.33	2.37
M123Q	4.18	2.47	1.99	2.04	2.31	2.37
M123L	2.59	2.49	2.00	2.05	2.32	2.37
M123H	2.36	2.50	2.04	2.05	2.35	2.36

* The unit of distance is in Å.

† The distance is average from two Cu_M-S and Cu_O-S distances, respectively.

Table S4. Calculated Cu-O (H_2O) and Cu_2S_2 core vibration modes (ν_2- ν_4) in M123L and their isotope shifts.

	M123L			
(cm^{-1})	Cu-O(H_2O)	ν_2	ν_3	ν_4
Cu-O($H_2{}^{16}O$)	108/116	239/250	272	338
Cu-O($D_2{}^{16}O$)	109/116	239/250	272	338
Cu-O($H_2{}^{18}O$)	106/113	239/250	272	338

Table S5. Calculated g_z and the σ^*_u to π_u transition energies and Cu characters in the donor (β) and acceptor (α) orbitals of WT and the M123X (X=Q, L, H) DFT models.

	WT	M123Q	M123L	M123H
g_z (calc.)-DFT	2.192	2.190	2.209	2.214
σ^*_u (α^2)	53	53	54	54
π_u (β^2)	28	29	30	30
ΔE (σ^*_u - π_u)	4639	4601	4478	3915
g_z (calc.)-Eq. 1*	2.21	2.22	2.24	2.27

* g_z-values were calculated using Eq 1 and the DFT derived ΔE, α^2, and β^2 values in this table. Note that these show the same trend as those obtained directly from the DFT calculation, which is also consistent with experiment.